



HAL
open science

Anhydrous alkali copper sulfates-a promising playground for new Cu 2+ oxide complexes: new Rb-analogues of fumarolic minerals related compounds

Oleg I Siidra, Diana O Nekrasova, Dmitry O Charkin, Anatoly N Zaitsev, Artem S Borisov, Marie Colmont, Olivier Mentré, Darya V Spiridonova

► To cite this version:

Oleg I Siidra, Diana O Nekrasova, Dmitry O Charkin, Anatoly N Zaitsev, Artem S Borisov, et al.. Anhydrous alkali copper sulfates-a promising playground for new Cu 2+ oxide complexes: new Rb-analogues of fumarolic minerals related compounds. Mineralogical Magazine, 2021, pp.1-15. 10.1180/mgm.2021.73 . hal-03438932

HAL Id: hal-03438932

<https://hal.science/hal-03438932>

Submitted on 22 Nov 2021

HAL is a multi-disciplinary open access archive for the deposit and dissemination of scientific research documents, whether they are published or not. The documents may come from teaching and research institutions in France or abroad, or from public or private research centers.

L'archive ouverte pluridisciplinaire **HAL**, est destinée au dépôt et à la diffusion de documents scientifiques de niveau recherche, publiés ou non, émanant des établissements d'enseignement et de recherche français ou étrangers, des laboratoires publics ou privés.

**Anhydrous alkali copper sulfates – a promising playground for new Cu²⁺ oxide complexes:
new Rb-analogues of fumarolic minerals related compounds.**

Oleg I. Siidra^{1,2*}, Diana O. Nekrasova^{1,3}, Dmitry O. Charkin⁴, Anatoly N. Zaitsev⁵, Artem S. Borisov^{1,5}, Marie Colmont³, Olivier Mentré³, Darya V. Spiridonova¹

¹*Department of Crystallography, St. Petersburg State University, University Embankment 7/9, 199034 St. Petersburg, Russia*

²*Kola Science Center, Russian Academy of Sciences, Apatity, 184200, Murmansk Region, Russia*

³*Université Lille, CNRS, Centrale Lille, Université Artois, UMR 8181, Unité de Catalyse et Chimie du Solide, Lille, F-59000, France*

⁴*Department of Chemistry, Moscow State University, GSP-1, Moscow 119991, Russia*

⁵*Department of Mineralogy, St. Petersburg State University, University Embankment 7/9, 199034 St. Petersburg, Russia*

* E-mail: o.siidra@spbu.ru

Abstract

Keywords: rubidium; sulfates; fumarolic minerals; solid state reactions; gas transport reactions; fumaroles; crystal structures

Introduction

10 years ago, the amount of structurally characterized anhydrous sulfates of copper and alkali metals was very limited. Most of the known compounds belonged to minerals from volcanic fumaroles. Euchlorine $\text{KNaCu}_3\text{O}(\text{SO}_4)_3$ (Scordari and Stasi, 1990; Siidra et al., 2019) and chlorothionite $\text{K}_2\text{Cu}(\text{SO}_4)\text{Cl}_2$ (Giacovazzo et al. 1976) were discovered more than a century ago on the fumaroles of Vesuvius volcano. Much later, after the Great Fissure Tolbachik Eruption in Kamchatka in 1975-1976, a large number of new endemic anhydrous copper sulfates were identified (Vergasova and Filatov, 2012). The overwhelming majority of the latter belonged to new structure types and had no known synthetic analogs. A well-known characteristic of transition metal sulfates is their excellent solubility and hydration in air with the appearance of a large number of reaction by-products. The latter requires special conditions during transportation and work in the laboratory. Despite a significant number of articles on copper and alkali metal sulfates that have appeared in the last few years, rubidium sulfates are almost unknown. It is known that, in the series of alkali metals from Na to Cs in the structures of oxides and oxysalts the phenomenon of morphotropism is commonly observed. As a rule, potassium and rubidium representatives are isostructural, while sodium and cesium ones can demonstrate own structure types.

The wave of interest in anhydrous transition metal sulfates and alkalis in the 2010s is associated with the search for novel electrode materials for possible application as cathodes in rechargeable metal-ion batteries (Masquelier and Croguennec, 2013). Sulfates represent a promising class of compounds for such applications given their superior electronegativity (Rousse and Tarascon, 2014).

In addition to experimental work on the synthesis of rubidium analogs of anhydrous potassium and sodium sulfates, one of the goals of this work was also an analysis and a brief review of the geochemistry of rubidium in volcanic environments. This is discussed in the chapter below.

Geochemistry of rubidium in volcanic environments

Quaternary arc volcanism on the Kamchatka peninsula, Russia, produced huge volume of basaltic rocks which form numerous large volcanoes and monogenetic volcanic fields. Among the

active volcanoes the most known and well studied is the Tolbachik volcanic complex; it is part of the Kluchevskaya Volcanic Group in Central Kamchatka Depression (Churikova et al 2015a and references herein). Tolbachik complex consists of two stratovolcanoes, extinct Ostry Tolbachik and active Plosky Tolbachik, and monogenetic volcanic field known as Tolbachinsky Dol. The latter was formed during several eruptions including Great Fissure Tolbachik Eruption in 1975–76 and Tolbachik fissure eruption in 2012–2013 (Volynets et al 2015).

The large volume of erupted lavas due to Tolbachik's recent activity are well studied in terms of their mineralogy and geochemistry, including direct sampling during eruptions. (Churikova et al 2015a and references herein). The Tolbachik lavas and scoria consist of basalts and basaltic andesites with subordinate trachybasalts and basaltic trachyandesite. Basalts, on the basis of potassium content, are subdivided into medium- and high-K varieties, and another basalt subdivision is based on MgO/Al₂O₃ ratio into high-magnesian, high-alumina and intermediate rocks. Published whole-rock geochemical data (e.g. Churikova et al 2015b, Portnyagin et al 2015, Volynets et al 2015) show large variations in content of both major and trace elements, e.g. MgO = 2.1-10.7 wt.%, Na₂O = 2.3-4.2 wt.%, K₂O = 0.7-3.1, Cr = 7-745 ppm. Unusual geochemical feature of the Tolbachik basalts is their enrichment in copper with 100-250 ppm in bulk rock samples (Portnyagin et al 2015). On multi-elements normalizing diagrams (relatively to N-type of mid-ocean ridge basalts) the Tolbachik basaltic rocks show enrichment in large ion lithophile elements (e.g. Cs, Rb, Ba) and depletion in high field strength elements (e.g. Nb, Ta). This is considered to be a typical signature of subduction related magmas (Churikova et al 2001). Mineralogy, trace element geochemistry and data from Sr–Nd–Pb isotopic studies suggest involvement of several components during formation of primary melts including subducted Pacific sediments, oceanic basaltic crust with additional fluid flux from subducted material (Churikova et al 2001 Portnyagin et al 2015) and even assimilation at crustal level of ore-bearing hydrothermal vein (Zelenski et al 2016).

Tolbachik is also well known due to strong fumarolic activity and remarkable mineralogy of fumarolic deposits. They have been studied since XXX and hundreds of new minerals with unusual combination of both abundant and trace elements have been found and described in details (references). Besides silicates, XXX, particularly abundant are sulfate minerals with Na and K as major cations. Other alkaline elements, Rb and Cs, are extremely rare in fumarolic minerals. XXX Yet, some species contain these elements in trace to minor amount (up to 1.95 wt.% Rb₂O in cesiodymite and 4.11 wt.% Cs₂O in averievite, Vergasova et al 1998, Pekov et al 2018) while cesiodymite, contains Cs as the major constituent (Pekov et al., 2018).

Rb, the element on which this paper is focused, is a trace element in Tolbachik basaltic rocks with concentration between 13 ppm (primitive high-Mg basalts) and 89 ppm (evolved low-Mg basaltic andesites) (references). Rb_N values (normalized relative to N-MORD) vary from 24 to 159.

On Harker-type diagrams, the element exhibits a clear positive correlation with K_2O (Supplementary Fig. 1) and this relationship seems to be common for the Quaternary volcanic rocks from Kurile-Kamchatka region (Popolitov, Volynets 1982). In basalts, Rb is likely to be hosted by plagioclase pheno- and microphenocrysts and possibly by the groundmass glass.

Rb is also present in high-temperature magmatic gases (1030-1060°C) sampled during 2012-13 eruption and considered to be uncontaminated. The measured Rb content in condensate is 1.0 ± 0.2 ppm (Zelenski et al 2014) and 1.7 ppm (Chaplygin et al 2016). A slightly lower concentration of Rb (0.78 ppm) was measured in the gases upon 1975-1976 eruption (Menyailov, Nikitina 1980). In contrast, the Rb content in the low-temperature gas (690 °C) from 2012-13 eruption was found as outstandingly high as 16.5 ppm (Chaplygin et al 2016). However, the strong gas enrichment in trace elements was explained as a secondary feature due to “evaporation at forced pumping during sampling and possible dissolution of earlier precipitated sublimates in the gas conduit” (Chaplygin et al 2016, p.186). Despite the low Rb content in Tolbachik gases, it is essentially above that in gases produced by other volcanoes. For instance, exhalations of Kudryavy (Kurily, Russia), Gorelyi (Kamchatka, Russia), Erta Ale (Afar, Ethiopia), Mount St. Helens USA) and White island (New Zealand) volcanoes exhibit extremely low Rb content in condensate with values between 0.22 and 0.002 ppm (Tedesco, Toutain 1991, Symonds, Reed 1993, Taran et al 1995, Wahrenberger et al 2002, Zelenski et al 2013, Chaplygin et al 2015). The high enrichment factor for Rb in Tolbachik gases ($\text{LogEF}_{\text{Rb}} = 2-3$, Chaplygin et al 2016, Zelenski et al 2013, 2014) suggests that the element was transported in the form of volatile species from a source and not derived from wall rocks due to contamination.

As yet, the compositional data on whole rock basalts with different degree of alteration by fumarolic gases are yet lacking and one can but suggest the tentative mechanisms of gas enrichment by the trace elements to the levels essential for the crystallization of Rb-enriched minerals. For instance, such strong Rb enrichment could be due to its extraction by hot hydrated gases from the plagioclase and glass, and/or dissolution of some earlier precipitated fumarolic minerals, e.g. sulfates, as suggested by Chaplygin et al (2016). In this case, some helpful data can be collected from the results of model experiments, including chemical composition, structure, formation mechanism (chemical transport, crystallization from melt, hydration rate etc.) and other features of synthetic Rb-containing species chemically relevant to the yet few known minerals. As yet, rubidium accumulates mostly in the copper sulfate/oxysulfate/halosulfate family, e.g. XXX (References). This approach is supported by our recent successful synthesis of Rb- and Cs-based analogs of mineral species, e.g. $M_2\text{Cu}_3\text{O}(\text{SO}_4)_3$ ($M = \text{Rb}, \text{Cs}$) as analogs of fedotovite ($M = \text{K}$) (Nekrasova et al. 2020). The current paper reports the results of our further studies of multinary Rb – Cu sulfates where no less than 8 new compounds representing 4 new structure types have been observed.

Experimental Section

Synthesis

In view of the fact that sulfate potassium-based minerals like chlorothionite $\text{K}_2\text{Cu}(\text{SO}_4)\text{Cl}_2$, piypite $\text{K}_4\text{Cu}_4\text{O}_2(\text{SO}_4)_4 \cdot (\text{Na,Cu})\text{Cl}$ and cryptochalcite $\text{K}_2\text{Cu}_5\text{O}(\text{SO}_4)_5$ were found in fumarolic sublimates, chemical vapor transport reactions method (CVT-method) was chosen due to similarity with natural conditions of mineral formation from volcanic gases. In our case, most reactions did not produce essential sublimates so we can consider the way of preparation as conventional solid-state synthesis in evacuated silica tubes.

Synthesis of $\text{Rb}_2\text{Cu}(\text{SO}_4)\text{Cl}_2$ and $\text{Rb}_4\text{Cu}_4\text{O}_2(\text{SO}_4)_4 \cdot (\text{Cu}_{0.83}\text{Rb}_{0.17}\text{Cl})$

Single crystals of $\text{Rb}_2\text{Cu}(\text{SO}_4)\text{Cl}_2$ and $\text{Rb}_4\text{Cu}_4\text{O}_2(\text{SO}_4)_4 \cdot (\text{Cu}_{0.83}\text{Rb}_{0.17}\text{Cl})$ were grown by slow cooling of melt containing of anhydrous CuSO_4 (Prolabo, 98%) and RbCl (Alfa Aesar, 99%) in ratio 1:2. The precursors were pre-dried at 200 °C for 2 h to remove traces of absorbed water and further rapidly mixed and ground in an agate mortar in air for 5 min. The mixtures were pressed into pellets (ca. 5 × 2 mm) and loaded into silica ampoules (ca. 10 × 0.8 cm), which were evacuated (10–2 mbar) and further sealed. The ampoules were placed horizontally in a tubular furnace and heated up to 700 °C for 3 hours and kept for 10 h. Cooling to 550°C was performed in 72 h, and in more 12 hours to room temperature. The products consisted of sky-blue crystals of $\text{Rb}_2\text{Cu}(\text{SO}_4)\text{Cl}_2$ and green ones of $\text{Rb}_4\text{Cu}_4\text{O}_2(\text{SO}_4)_4 \cdot (\text{Cu}_{0.83}\text{Rb}_{0.17}\text{Cl})$ (Fig.1).

Synthesis of $\text{Rb}_2\text{Cu}_2(\text{SO}_4)_3$ and $\text{Rb}_2\text{Cu}_5\text{O}(\text{SO}_4)_5$

Crystals of $\text{Rb}_2\text{Cu}_2(\text{SO}_4)_3$ and $\text{Rb}_2\text{Cu}_5\text{O}(\text{SO}_4)_5$ were formed in the same experimental run. Rb_2SO_4 (Sigma-Aldrich, 99.99%) and CuSO_4 (Prolabo, 98%) were mixed carefully in an agate mortar in ratio 3:1, pelletized, and sealed as described above. The ampoule was heated up to 700 °C for 3 hours soaked for 10 h, cooled to 500 °C in 96 h and further in 12 h to room temperature. The products consisted of green $\text{Rb}_2\text{Cu}_5\text{O}(\text{SO}_4)_5$ and sky-blue $\text{Rb}_2\text{Cu}_2(\text{SO}_4)_3$ crystals (Fig.1)

Synthesis of $\text{Rb}_2\text{Cu}_2(\text{SO}_4)_3(\text{H}_2\text{O})$

The new compound $\text{Rb}_2\text{Cu}_2(\text{SO}_4)_3(\text{H}_2\text{O})$ was synthesized during a side process. A 3:1 mixture of Rb_2SO_4 (Sigma-Aldrich, 99.99%) and CuSO_4 (Prolabo, 98%) was accidentally exposed to air for one week. The color of the mixture turned light blue due to hydration of copper sulfate. The mixture was processed as described above; the ampoule was heated to 750 °C in 5 h, soaked for 10 h, then cooled to 500 °C on 40 h after which the furnace was switched off. The products consisted of green crystals of $\text{Rb}_2\text{Cu}_5\text{O}(\text{SO}_4)_5$ and light-blue crystals of $\text{Rb}_2\text{Cu}_2(\text{SO}_4)_3(\text{H}_2\text{O})$.

Synthesis of $RbMCu(SO_4)_2$ ($M = Na, K, Rb$)

The new compounds were prepared according to a slightly different protocol. Mixtures of Rb_2SO_4 , Na_2SO_4 or K_2SO_4 (all pre-heated at 140°C for 3-4 hrs) and $CuSO_4$ (obtained by dehydration of $CuSO_4 \cdot 5H_2O$ at 450°C for 4 hrs) were taken in 1:1:2 molar ratio, ground and placed in silica capsules (5 mm inner diameter, 100 mm length). The tubes were evacuated to $3 \cdot 10^{-2}$ Torr, flame sealed and placed in a vertical furnace with “cold” ends protruding out so that any absorbed water would condense therein. The mixtures were annealed first at 350°C for 96 hrs; the ampoules were opened, inhomogeneous samples re-ground and further annealed at $450\text{--}475^\circ\text{C}$ for more 96 hrs. The samples partially melted and formation of green or blue crystals was observed.

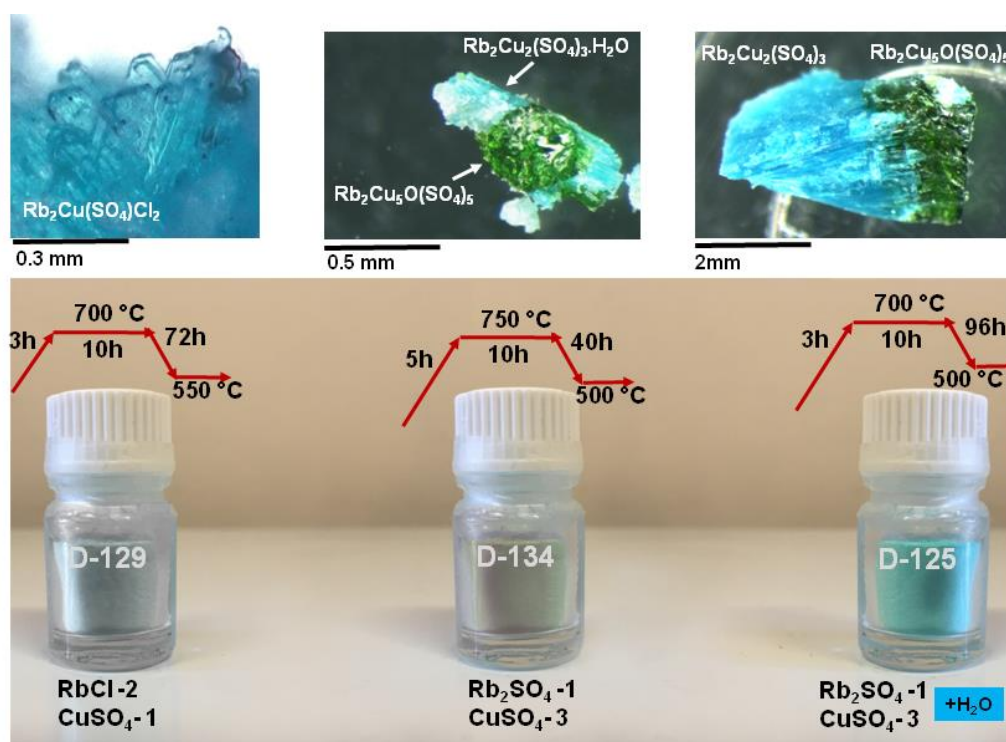


Figure 1. Crystals of blue $Rb_2Cu(SO_4)Cl_2$, green $Rb_2Cu_5O(SO_4)_5$, blue $Rb_2Cu_2(SO_4)_3 \cdot H_2O$ and $Rb_2Cu_2(SO_4)_3$ crystals. Initial reagent mixtures and schemes of the synthesis for each compound.

Single-crystal X-ray studies.

Single crystals of all compounds were visually checked under microscope and mounted on thin glass fibers for X-ray diffraction analysis using Bruker APEX II DUO X-ray diffractometer with a micro-focus X-ray tube operated with $MoK\alpha$ radiation at 50 kV and 0.6 mA. The data were integrated and corrected for absorption using a multi scan type model using the Bruker programs *APEX* and *SADABS* (Bruker, 2014). More than a hemisphere of X-ray diffraction data was collected for each crystal. The structure refinements were performed using *SHELXL* software (Sheldrick,

2015). Crystallographic information for all obtained phases is summarized in Table 1. Atomic coordinates and additional structural information are provided in the Supporting Information (CIF).

3. Results

3.1 Structures without additional O²⁻ anions.

Rb₂Cu(SO₄)₂

Statistics of diffraction intensities and systematic extinctions were consistent with the space group *Pna2₁*. The $|E^2-1|$ parameter was equal to 0.668, which clearly indicated high probability of a non-centrosymmetric space group (Marsh, 1995) confirmed by subsequent structure solution and refinement.

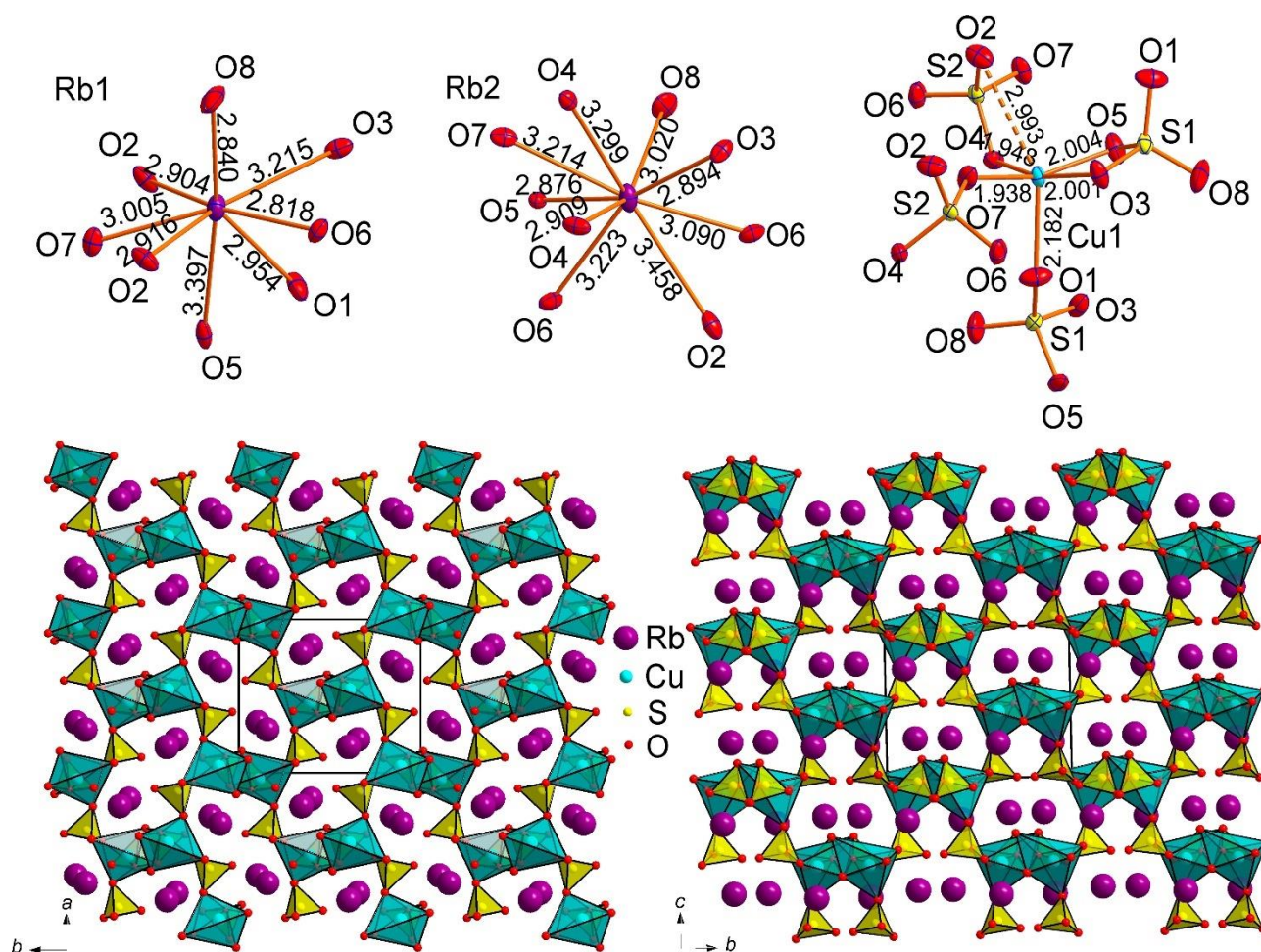


Figure 2. Coordination environments of Rb⁺, Cu²⁺ and S⁶⁺ cations (above) in the crystal structure of Rb₂Cu(SO₄)₂. General projections of the crystal structure of Rb₂Cu(SO₄)₂ along the *c* and *a* axis, respectively (below).

The structure contains respectively one symmetrically independent Cu²⁺, two Rb⁺ and two S⁶⁺ cations. All Cu-O bonds ≤ 3.05 Å and Rb-O bonds ≤ 3.55 Å were taken into consideration. Cu1 atom forms four very strong Cu-O_{eq} bonds (≤ 2 Å) resulting in CuO₄ square which is complemented by a

fifth, longer Cu-O_{ap} bond of 2.182 Å, to form CuO₅ distorted tetragonal pyramid (Figure 2). The copper atom forms one additional very weak bond of 2.994(4) Å resulting in [4+1+1] CuO₆ octahedron strongly distorted by the Jahn-Teller effect. This type of coordination geometry of Cu²⁺ cations is rather common in minerals and inorganic materials (Burns and Hawthorne 1996).

Both Rb cations center irregular polyhedra of oxygen atoms (8 vertices for Rb1 atom and 9 for Rb2). Each of two S sites centers the respective tetrahedra. The average S-O bond-lengths, 1.47 Å, are consistent with the value of 1.475 Å given for sulfate minerals in general (Hawthorne et al. 2000).

The CuO₆ polyhedra share O3-O5 and O4-O5 oxygen edges and O1, O7 vertices with SO₄ tetrahedra forming clusters depicted in Figure 2. These are linked into an open framework with three-dimensional system of channels occupied by the Rb⁺ cations. The structural topology of the [Cu(SO₄)₂]²⁻ framework in Rb₂Cu(SO₄)₂ is unique and has not been observed before.

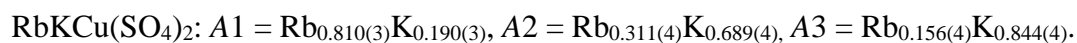
The Cu1-S1 and Cu1-S2 distances in Rb₂Cu(SO₄)₂ are 2.5718(13) Å and 2.9737(12) Å, respectively. In fact, edge sharing between sulfate tetrahedra and transition metal octahedra is rather uncommon. A similarly short Cu-S distance of 2.593 Å is observed in chlorothionite, K₂CuCl₂(SO₄) (Giacovazzo et al., 1976) wherein the CuO₆ octahedron shares an edge with a SO₄ group. Edge sharing has also been recently observed in a complex Zn sulfate majzlanite, K₂Na(ZnNa)Ca(SO₄)₄ (Siidra et al., 2020), with the Zn-S distance of 2.8704(4) Å.

RbNaCu(SO₄)₂ and RbKCu(SO₄)₂

Both structures contain each one symmetrically independent Cu site, two S sites and three A (A = Rb, K, Na) sites (Figure 3).

The Cu²⁺ cation is coordinated by the four Cu-O_{eq} short bonds with distances around 2 Å and forming a nearly square planar coordination. The lengths of the fifth (longer) Cu-O_{ap} differ essentially: 2.236(2) Å in RbNaCu(SO₄)₂ while 2.547(3) Å in RbKCu(SO₄)₂. The effect of the alkali cation size on the Cu²⁺ coordination has been observed before in layered copper hydrogen selenite halides (Charkin et al. 2019). The CuO₅ tetragonal pyramids are complemented by the sixth long and relatively weak bond of 2.604(2) Å and 2.713(3) Å for RbNaCu(SO₄)₂ and RbKCu(SO₄)₂, respectively. Thus, the coordination polyhedron of Cu²⁺ cation can be also described as [4+1+1].

In contrast to KNaCu(SO₄)₂, the cation ordering in the rubidium analog is less perfect. Only A1 site in the sodium compound is occupied exclusively by Rb⁺ while the other alkali sites demonstrate mixed occupancies:



The A2 and A3 sites in RbNaCu(SO₄)₂ contain only minor amount of Rb⁺ admixture. The coordination environments for these sites are typical for Na⁺ cations (distorted octahedra, Figure 3), while CN =

11 of A1 site is typical for Rb^+ . In $\text{RbKCu}(\text{SO}_4)_2$, the A2 and A3 sites correspond to coordination numbers (CN=10 for both sites) in accordance with larger radius of K^+ . In this case, cation disorder is more pronounced which agrees with the smaller relative differences in cation size.

The S atoms center approximately regular SO_4 tetrahedra. Akin to $\text{Rb}_2\text{Cu}(\text{SO}_4)_2$, the sulfate moieties share one of the edges with CuO_6 octahedra ($\text{Cu-S} = 2.8315(8) \text{ \AA}$ and $2.8756(11) \text{ \AA}$ for $\text{RbNaCu}(\text{SO}_4)_2$ and $\text{RbKCu}(\text{SO}_4)_2$, respectively) (Figure 3), despite unfavourable repulsive interactions between the Cu^{2+} and S^{6+} .

$\text{RbNaCu}(\text{SO}_4)_2$ and $\text{RbKCu}(\text{SO}_4)_2$ are formally isostructural to the recently reported $\text{KNaCu}(\text{SO}_4)_2$ (Borisov et al., 2021) and $\text{K}_2\text{Cu}(\text{SO}_4)_2$ (Zhou et al., 2020), though some differences in the cation coordinations are clearly visible. The SO_4 tetrahedra and the CuO_6 polyhedra form the porous $[\text{Cu}(\text{SO}_4)_2]^{2-}$ framework with two types of channels parallel to the c axis. The larger (elliptical) channels are occupied preferably by larger Rb^+ (A1 sites), whereas the smaller ones are filled mostly by Na^+ (in $\text{RbNaCu}(\text{SO}_4)_2$) or K^+ (in $\text{RbKCu}(\text{SO}_4)_2$). Note the complete size-derived ordering of alkali cations in $\text{KNaCu}(\text{SO}_4)_2$ (Borisov et al., 2021), which is somewhat smeared in its Rb-based analogs.

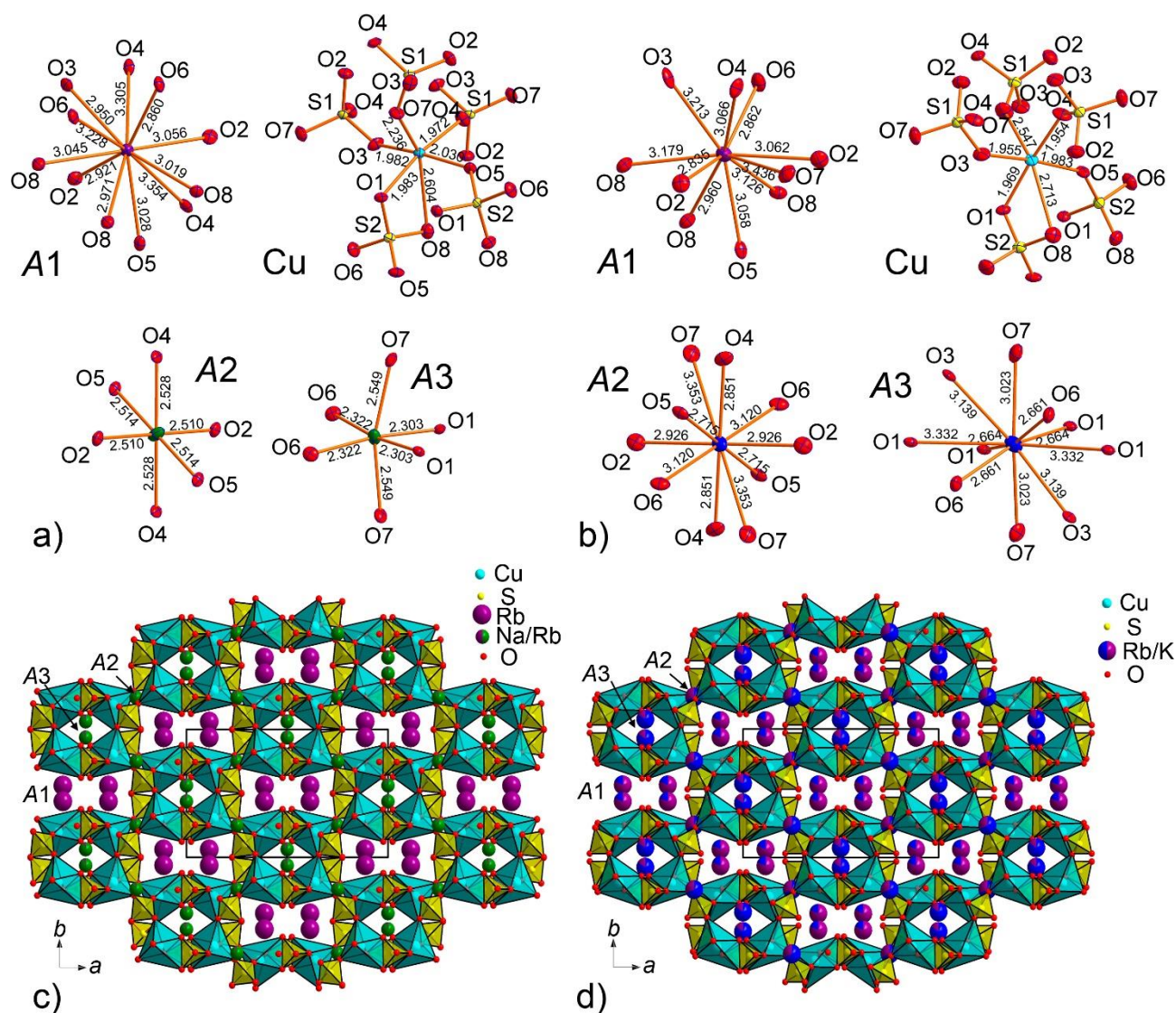
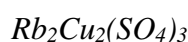


Figure 3. Coordination environments of A^+ ($A = \text{Rb}, \text{K}, \text{Na}$), Cu^{2+} and S^{6+} cations in the crystal structures of $\text{RbNaCu}(\text{SO}_4)_2$ (a) and $\text{RbKCu}(\text{SO}_4)_2$ (b). General projections of the crystal structure of $\text{RbNaCu}(\text{SO}_4)_2$ (c) and $\text{RbKCu}(\text{SO}_4)_2$ (d) along the c axis.



The crystal structure of another new anhydrous sulfate with langbeinite $A^+_2M^{2+}_2(\text{SO}_4)_3$ stoichiometry contains two symmetrically independent Rb sites, two Cu sites and three S atoms (Figure 4).

In $\text{Rb}_2\text{Cu}_2(\text{SO}_4)_3$, Rb^+ and S^{6+} cations have typical and similar to the described above coordination environments, whereas coordination of Cu^{2+} cations demonstrate interesting features worthy of discussion. Cu1 atom has four short and strong Cu-O_{eq} bonds thus forming CuO₄ squares. However, it has three additional very long Cu1-O5 = 2.864(12), Cu1-O1 = 2.925(15) Å and Cu1-O10 = 2.981(15) Å bonds, thus forming [4+3] coordination environments. These Cu-O bonds have bond-valence sums of 0.04-0.03 *v.u.* and thus should be taken into consideration. Cu2 atom has CuO₆

[4+1+1] coordination environments described above in $\text{Rb}_2\text{Cu}(\text{SO}_4)_2$. Both, CuO_6 and CuO_7 polyhedra demonstrate bidentate bridging with SO_4 tetrahedra.

$\text{Rb}_2\text{Cu}_2(\text{SO}_4)_3$ is isostructural to $\text{K}_2\text{Cu}_2(\text{SO}_4)_3$ described by Lander et al. (2017). The Cu-centered polyhedra and SO_4 tetrahedra form $[\text{Cu}_2(\text{SO}_4)_3]^{2-}$ bands depicted in Figure 4. The arrangement of sulfate tetrahedra and Cu-centered polyhedra was originally described by Lander et al. (2017) as a herringbone pattern.

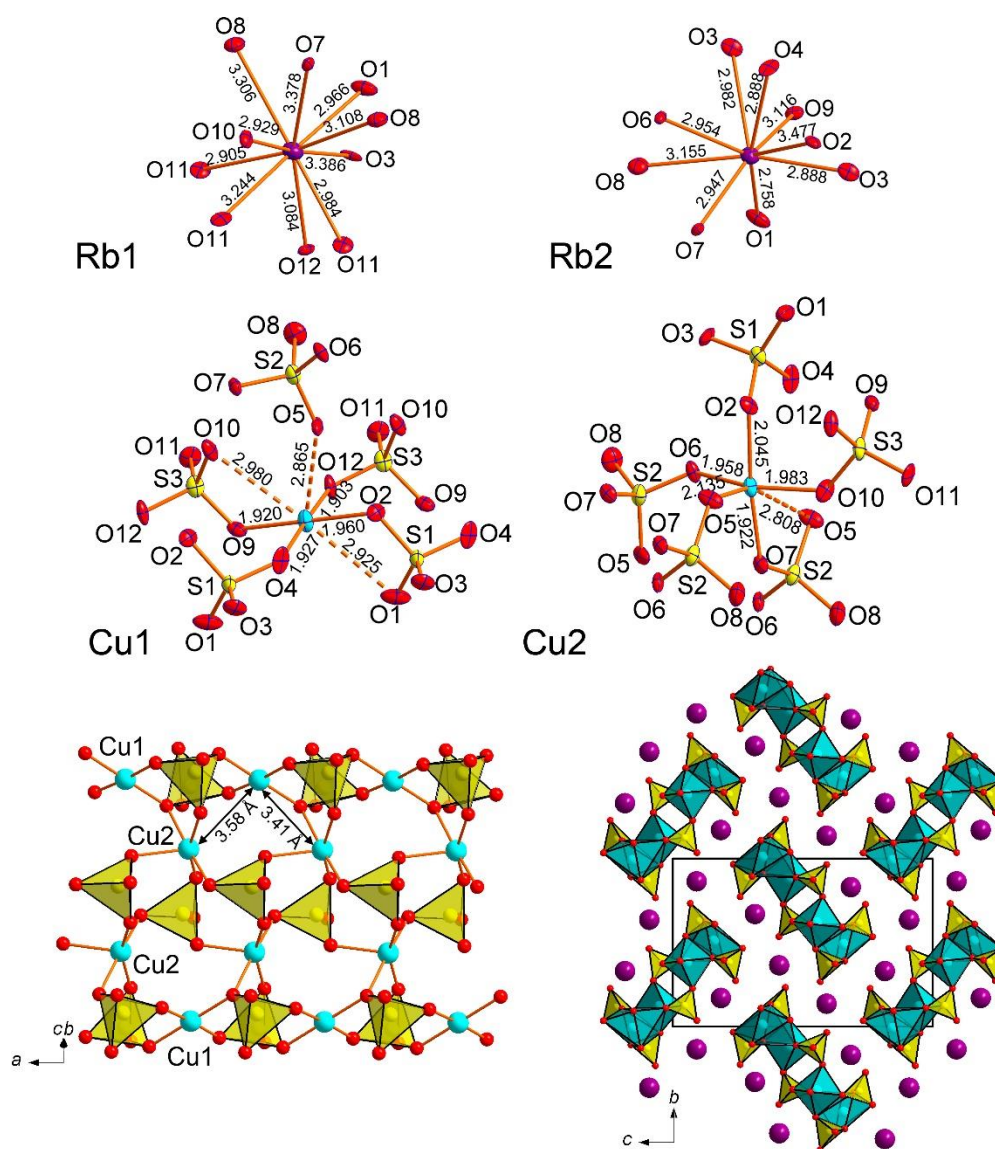


Figure 4. Coordination environments of Rb^+ , Cu^{2+} and S^{6+} cations (above) in the crystal structure of $\text{Rb}_2\text{Cu}_2(\text{SO}_4)_3$. $[\text{Cu}_2(\text{SO}_4)_3]^{2-}$ band (only short and strong Cu-O bonds are shown) (left below) and general projection of the crystal structure of $\text{Rb}_2\text{Cu}_2(\text{SO}_4)_3$ along the a axis (right below).

$\text{Rb}_2\text{Cu}_2(\text{SO}_4)_3(\text{H}_2\text{O})$ “hydrolangbeinite”

The dominant motif of the $\text{Rb}_2\text{Cu}_2(\text{SO}_4)_3(\text{H}_2\text{O})$ structure are layers formed by the corner sharing and edge-sharing between sulfate tetrahedra and copper polyhedra (Figure 5). The $[\text{Cu}_2(\text{SO}_4)_3(\text{H}_2\text{O})]^{2-}$ layers are parallel to the ab plane. In general, layered character is typical for

hydrated copper oxysalt structures. In $\text{Rb}_2\text{Cu}_2(\text{SO}_4)_3(\text{H}_2\text{O})$, the layers are linked together by Rb1 and Rb2 atoms coordinated by the eight and ten oxygen anions, respectively. Note, water molecules are bonded exclusively to Rb1 atoms. The Cu1 site shows typical coordination with the formation of CuO_5 tetragonal pyramids with almost planar CuO_4 base. Cu2-centered CuO_6 octahedron demonstrates exceptionally strongly distorted character. Cu2-O5 and Cu2-O6 bonds are strongly inclined (Figure 5) relative to the equatorial plane of octahedron. This distortion is again due to the edge-sharing through O5-O6 with S_2O_4 tetrahedron. The topology of $[\text{Cu}_2(\text{SO}_4)_3(\text{H}_2\text{O})]^{2-}$ layer is somewhat similar to that one for the $[\text{Cu}_2(\text{SO}_4)_3]^{2-}$ bands in anhydrous $\text{Rb}_2\text{Cu}_2(\text{SO}_4)_3$ (Figure 4). The rearrangement of sulfate groups in $\text{Rb}_2\text{Cu}_2(\text{SO}_4)_3(\text{H}_2\text{O})$ is provoked by the hydration of one of the Cu-centered polyhedra. The vertex occupied by the water molecule is unshared and projected into the interlayer space.

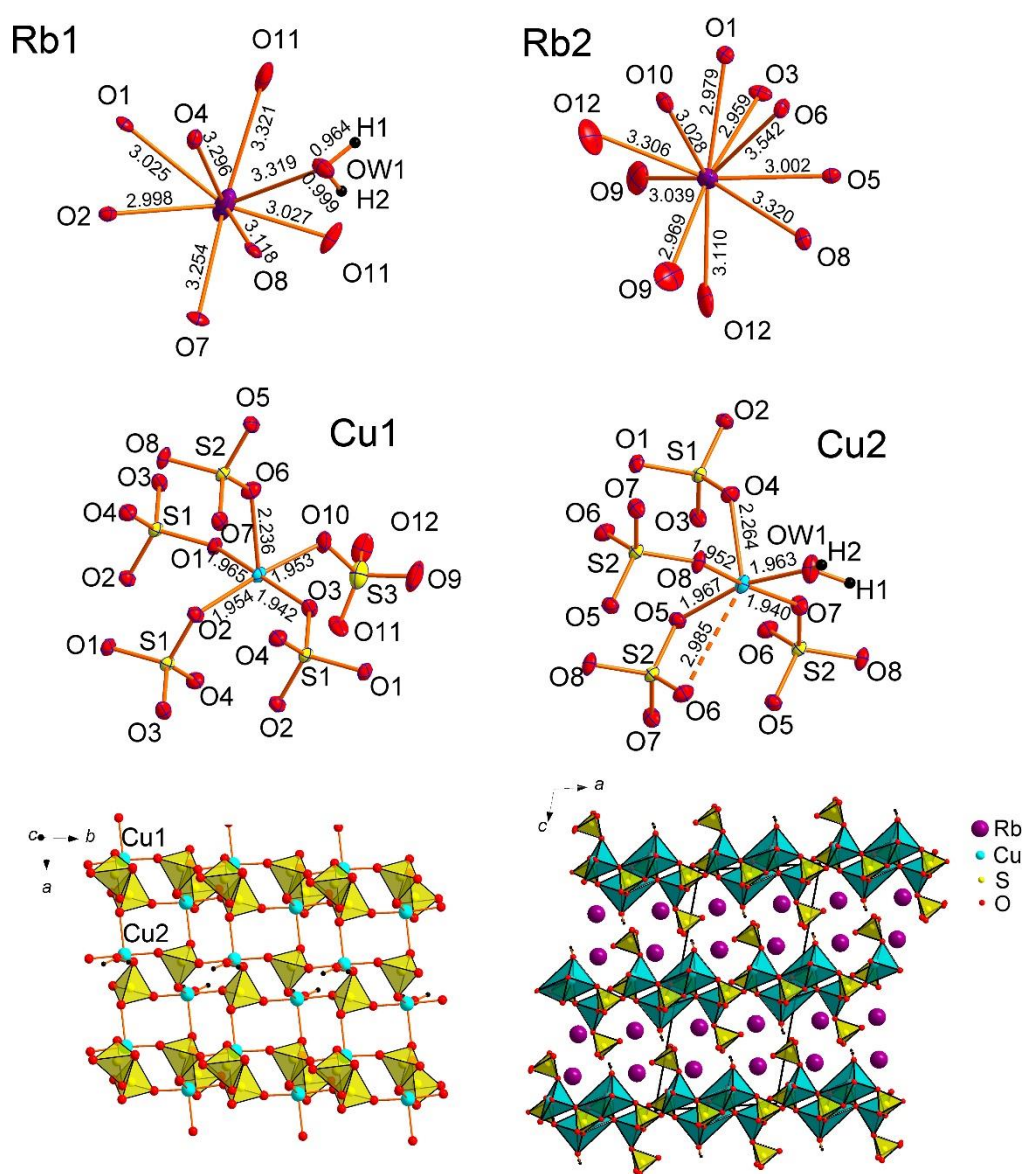


Figure 5. Coordination environments of Rb^+ , Cu^{2+} and S^{6+} cations (above) in the crystal structure of $\text{Rb}_2\text{Cu}_2(\text{SO}_4)_3(\text{H}_2\text{O})$. $[\text{Cu}_2(\text{SO}_4)_3(\text{H}_2\text{O})]^{2-}$ layer (only short and strong Cu-O bonds are shown) (left

below) and general projection of the crystal structure of $\text{Rb}_2\text{Cu}_2(\text{SO}_4)_3(\text{H}_2\text{O})$ along the b axis (right below).

Rb₂Cu(SO₄)Cl₂

The coordination environments of atoms in monoclinic ($C2/c$) $\text{Rb}_2\text{Cu}(\text{SO}_4)\text{Cl}_2$ are very similar to those described earlier in its natural analog, chlorotitionite $\text{K}_2\text{Cu}(\text{SO}_4)\text{Cl}_2$ (Giacovazzo *et al.*, 1976) crystallizing in orthorhombic $Pnma$ space group. The Cu atom demonstrates mixed-ligand coordination environments with oxygen and chlorine atoms thus forming the CuO_2Cl_2 coordination environments complemented by the two very long Cu-Cl bonds of 3.2020(8) Å (Figure 6). These Cu-Cl bonds are much shorter in chlorotitionite $\text{K}_2\text{Cu}(\text{SO}_4)\text{Cl}_2$ (3.0467(2) Å). The SO_4 tetrahedra in $\text{Rb}_2\text{Cu}(\text{SO}_4)\text{Cl}_2$ and $\text{K}_2\text{Cu}(\text{SO}_4)\text{Cl}_2$ show very similar S-O bond length values. Two symmetrically independent Rb atoms have strongly dissimilar coordination environments: $\text{Rb1O}_4\text{Cl}_4$ and Rb2O_4 . Rb2 has two Rb-Cl distances of 3.6652(10) Å and two of 3.6908(9) Å which are beyond the limit of 3.55 Å for the consideration of bonds. We should note also the unusually low coordination number of K in chlorotitionite.

In $\text{Rb}_2\text{Cu}(\text{SO}_4)\text{Cl}_2$, the main structural feature of edge sharing between sulfate tetrahedra and CuO_2Cl_4 octahedra remains intact. The Cu-S1 distances are 2.5785(10) Å and 2.593(1) Å in $\text{Rb}_2\text{Cu}(\text{SO}_4)\text{Cl}_2$ and chlorotitionite $\text{K}_2\text{Cu}(\text{SO}_4)\text{Cl}_2$, respectively.

The observed symmetry lowering in $\text{Rb}_2\text{Cu}(\text{SO}_4)\text{Cl}_2$ compared to $\text{K}_2\text{Cu}(\text{SO}_4)\text{Cl}_2$ is likely due to the replacement of K^+ by larger Rb^+ . This causes also the significant elongation of Cu-Cl bonds in the CuO_4Cl_2 octahedra.

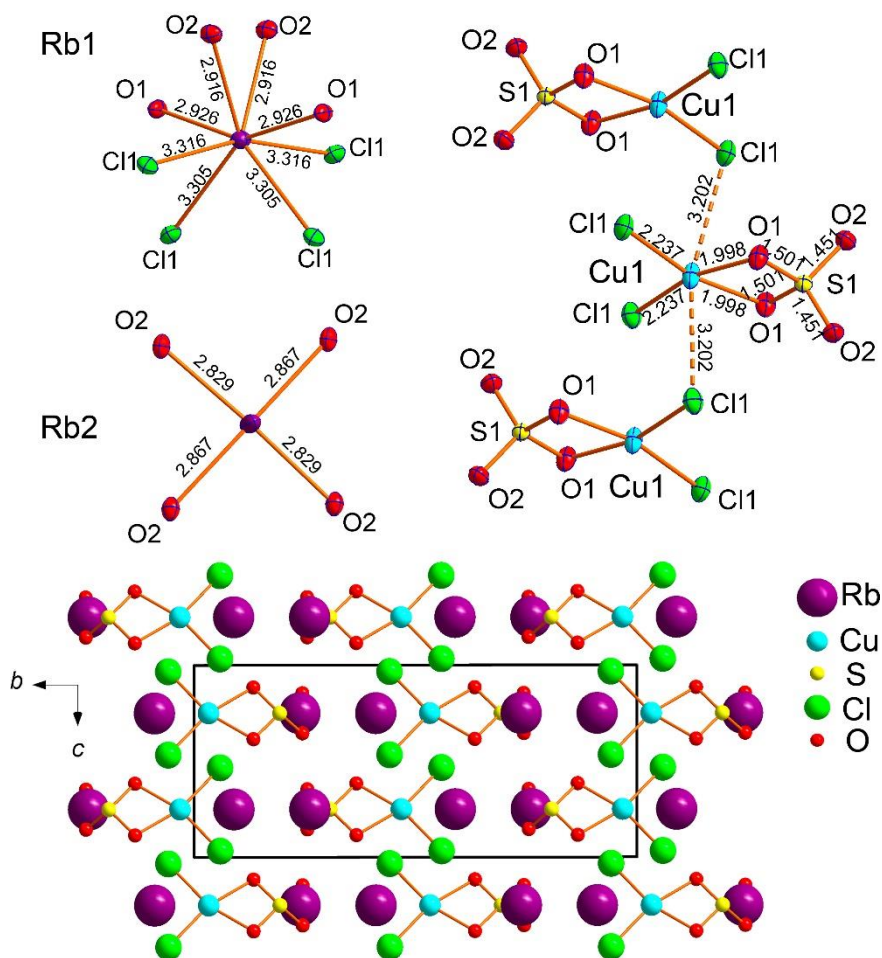


Figure 6. Coordination environments of Rb^+ , Cu^{2+} and S^{6+} cations (above) in the crystal structure of $\text{Rb}_2\text{Cu}(\text{SO}_4)\text{Cl}_2$. General projection of the crystal structure of $\text{Rb}_2\text{Cu}(\text{SO}_4)\text{Cl}_2$ along the a axis (below). Weak and long Cu-Cl bonds are not shown for clarity.

3.2 Structures with additional O^{2-} anions.

$\text{Rb}_4\text{Cu}_4\text{O}_2(\text{SO}_4)_4 \cdot (\text{Cu}^{+}_{0.83}\text{Rb}_{0.17}\text{Cl})$, rubidium analogue of piypite

Piypite $\text{K}_4\text{Cu}_4\text{O}_2(\text{SO}_4)_4 \cdot (\text{Na,Cu})\text{Cl}$ was described from the fumaroles of the Second scoria cone by Vergasova et al. (1984). The crystal structure was solved ($R_1 = 0.035$) on a sample of “caratiite” from Mount Vesuvius, Naples, Italy by Effenberger and Zemann (1984). It belongs to the tetragonal symmetry, $I4$, $a = 13.60(2) \text{ \AA}$, $c = 4.98(1) \text{ \AA}$, $V = 921.1 \text{ \AA}^3$. Later, Kahlenberg et al. (2000) solved the structure ($R_1 = 0.028$) of its synthetic sodium analog, $\text{Na}_4\text{Cu}_4\text{O}_2(\text{SO}_4)_4 \cdot (M\text{Cl})$ ($M = \text{Na}, \text{Cu}, \square$) in the supercell with $P4/n$, $a = 18.451(1)$, $c = 4.9520(2)$, and $V = 1685.86 \text{ \AA}^3$.

The new compound $\text{Rb}_4\text{Cu}_4\text{O}_2(\text{SO}_4)_4 \cdot (\text{Cu}_{0.83}\text{Rb}_{0.17}\text{Cl})$ crystallizes analogous to the potassium compound in space group in $I4$, $a = 14.171(14)$, $c = 4.991(5)$, $V = 1002(2) \text{ \AA}^3$, $R_1 = 0.043$. Proceeding from K to Rb, the value of the a parameter is affected most. We did not observe indication of the supercell suggested by Kahlenberg et al. (2000). In the structure of $\text{Rb}_4\text{Cu}_4\text{O}_2(\text{SO}_4)_4 \cdot (\text{Cu}_{0.83}\text{Rb}_{0.17}\text{Cl})$,

chlorine is disordered over two C11A (s.o.f. = 0.44(7)) and C11B (s.o.f. = 0.55(7)) sites with C11A-C11B = 0.82(2) Å. All of the atoms except of ClA were refined anisotropically.

The structure of $\text{Rb}_4\text{Cu}_4\text{O}_2(\text{SO}_4)_4(\text{Cu}_{0.83}\text{Rb}_{0.17}\text{Cl})$ (Figure 7) contains one symmetrically unique Rb position, one Cu, one S and one mixed metal site *M*, occupied by Cu^+ and Rb^+ cations in a ratio indicated above. The Rb^+ cation is coordinated by seven O atoms and two Cl atoms. The Cu site is coordinated by four oxygens forming a distorted CuO_4 square complemented by one apical O^{2-} anion at a distance of 2.395(8) Å and another one at 3.086(11) Å. As a result, an essentially elongated CuO_6 octahedron is formed.

The mixed *M* site has a refined occupancy of $\text{Cu}^{1_{0.83(7)}\text{Rb}_{0.17(7)}}$. There are two strong bonds to the Cl atoms ($M\text{-Cl1A} = 2.08(5)$ Å and $M\text{-Cl1B} = 2.09(3)$ Å) which correspond to a typical linear Cu^+Cl_2^- anion. There are also four equivalent *M*-O2 distances of 2.900(9) Å which transform into real bonds around Rb^+ .

The O1, O2, O3 and O4 oxygens constitute the tetrahedral SO_4^{2-} groups and are further termed as O_t . The “additional” O5 oxygen atom is bonded exclusively to the Cu^{2+} cations (Figure 7) and can be designated as O_a . The $\text{Cu}^{2+}\text{-O}_a$ distances vary in the range of 1.908(15) – 1.922(15) Å, whereas $\text{Cu}^{2+}\text{-O}_t$, from 1.908(15) to 3.086(11) Å. Because of the higher strength of the $\text{Cu}\text{-O}_a$ bonds compared to the weaker $\text{Cu}\text{-O}_t$, one can describe the copper-oxide substructure of $\text{Rb}_4\text{Cu}_4\text{O}_2(\text{SO}_4)_4(\text{Cu}_{0.83}\text{Rb}_{0.17}\text{Cl})$ in the terms of oxocentered OCu^{2+}_4 tetrahedra.

These tetrahedra link together via common edges to form the $[\text{O}_2\text{Cu}]^{2+}$ single chains (Figure 7). In such units, each tetrahedron shares two of six edges with adjacent tetrahedra. The $[\text{O}_2\text{Cu}]^{2+}$ single chains extend along the *c* axis. The chains are surrounded by SO_4 tetrahedra in a rod-like arrangement. Rb^+ cations fill the space in between the rods. In turn, the channels filled by CuCl_2^- linear complexes, are formed between the rubidium atoms. Formation of “guest” metal-chloride species with copper in the channels is characteristic for fumarolic minerals: averievite $\text{Cu}_5\text{O}_2(\text{VO}_4)\cdot n\text{MCl}_x$ ($M=\text{Cu}, \text{Cs}, \text{Rb}, \text{K}$) (Vergasova *et al.*, 1998; Korniyakov *et al.*, 2021) and aleutite $[\text{Cu}_5\text{O}_2](\text{AsO}_4)(\text{VO}_4)\cdot(\text{Cu}_{0.5}\square_{0.5})\text{Cl}$ (Siidra *et al.*, 2019). A similar phenomenon was observed in the family of copper-lead selenite bromides (Siidra *et al.* 2018): the oxocentered $\text{OCu}^{2+}_n\text{Pb}_{4-n}$ tetrahedra were present only in the structures containing both Cu^{2+} and Cu^+ . Whenever Cu^{2+} was the sole copper species, the anionic sublattice was formed only by SeO_3^{2-} and Br^- with no “extra” O^{2-} present. A possible explanation, which evidently needs to be further verified, is that the Cu^+ form strong covalent bonds to the halide anions. The terminal atoms of the strong halo- and/or oxoanions form weaker bonds to the dications (Pb^{2+} or Cu^{2+}) and the “extra” O^{2-} anions are one of the ways to complete their bond valence sums to saturation.

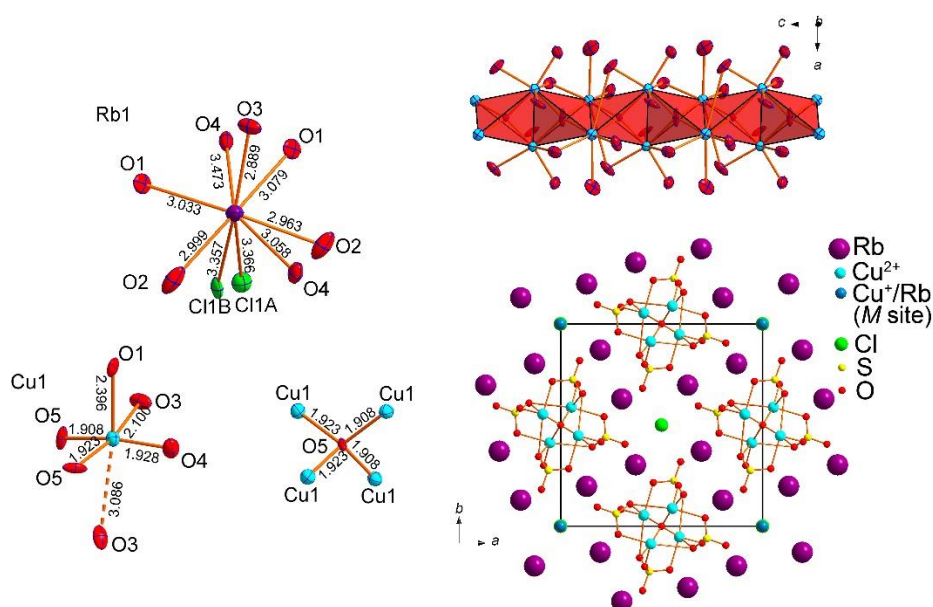


Figure 7. Coordination environments of Rb^+ , Cu^{2+} cations and additional O^{2-} anions cations in the crystal structure of $\text{Rb}_4\text{Cu}_4\text{O}_2(\text{SO}_4)_4 \cdot (\text{Cu}_{0.83}\text{Rb}_{0.17}\text{Cl})$ (left). Polyhedral representation of the oxocentered $[\text{Cu}_2\text{O}]^{2+}$ chains surrounded by the oxygen atoms of sulfate groups (right above). General projection of the crystal structure of $\text{Rb}_4\text{Cu}_4\text{O}_2(\text{SO}_4)_4 \cdot (\text{Cu}_{0.83}\text{Rb}_{0.17}\text{Cl})$ along the c axis (below) ($\text{Rb}-\text{Cl}$ and $M-\text{Cl}$, $M-\text{O}$ bonds are omitted for clarity).

$\text{Rb}_2\text{Cu}_5\text{O}(\text{SO}_4)_5$, rubidium analogue of cryptochalcite and cesiodymite

$\text{Rb}_2\text{Cu}_5\text{O}(\text{SO}_4)_5$ is isostructural to the recently described cryptochalcite, $\text{K}_2\text{Cu}_5\text{O}(\text{SO}_4)_5$, and cesiodymite $\text{CsKCu}_5\text{O}(\text{SO}_4)_5$ (Pekov et al., 2018). Note, both these fumarolic minerals contain significant amounts of Rb (up to 1.95 wt. % Rb_2O). The new compound $\text{Rb}_2\text{Cu}_5\text{O}(\text{SO}_4)_5$ is the first synthetic representative of this structure type. The initial model started from the atomic coordinates provided by Pekov et al. (2018). The unit-cell volume of $\text{Rb}_2\text{Cu}_5\text{O}(\text{SO}_4)_5$ ($V = 1770.9(3) \text{ \AA}^3$) is nearly halfway between those of cryptochalcite ($V = 1751.73(10) \text{ \AA}^3$) and cesiodymite ($V = 1797.52(16) \text{ \AA}^3$). The structure of cryptochalcite-type compounds, and $\text{Rb}_2\text{Cu}_5\text{O}(\text{SO}_4)_5$ in particular, represents an interesting example of the framework formed by both CuO_n copper-centered polyhedra and oxocentered OCu_4 tetrahedra. The $[\text{Cu}_5\text{O}(\text{SO}_4)_5]^{2-}$ open framework, with Rb^+ in the channels, can be described as consisting of two types of blocks, *A* and *B* (Figure 8). The *A*-blocks (in the middle) are formed by O_2Cu_6 dimeric units and sulfate tetrahedral, whereas *B*-blocks (right) are formed by CuO_5 tetragonal pyramids and sulfate tetrahedra.

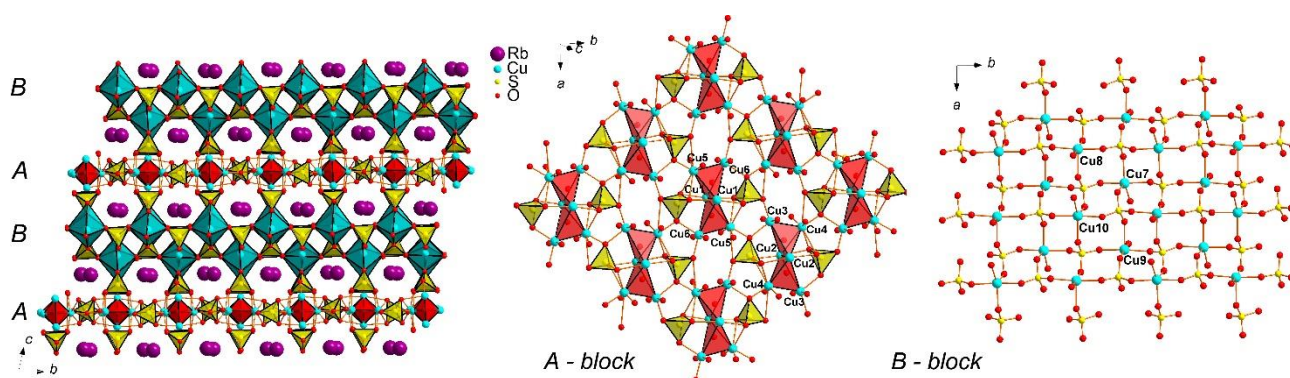


Figure 8. General projection of the crystal structure of $\text{Rb}_2\text{Cu}_5\text{O}(\text{SO}_4)_5$ along the a axis. The $[\text{Cu}_5\text{O}(\text{SO}_4)_5]^{2-}$ open-framework can be described as consisting of two types of blocks, A and B. A-blocks (in the middle) are formed by O_2Cu_6 dimeric units and sulfate tetrahedral, whereas B-blocks (right) are formed by CuO_5 tetragonal pyramids and sulfate tetrahedra. Rb-O bonds are omitted for clarity.

Discussion and concluding remarks

The new compounds obtained for the first time and the determination of their crystal structures significantly expand the family of anhydrous copper sulfates. Some of the obtained anhydrous rubidium copper sulfates turned out to be isostructural to known compounds and minerals. An example of this is $\text{Rb}_2\text{Cu}_5\text{O}(\text{SO}_4)_5$, which is completely isostructural to cesiodymite $\text{CsKCu}_5\text{O}(\text{SO}_4)_5$ and cryptochalcite $\text{K}_2\text{Cu}_5\text{O}(\text{SO}_4)_5$ (Table 2). This fact, as well as the high content of rubidium in natural samples, shows that the discovery of a mineral species with an alkali position, occupied essentially or even predominantly by rubidium, is highly probable. Our synthesis of a number of mineral analogs also demonstrates the possibility of introducing rubidium cations into the already known structural architectures. A slight symmetry lowering, with the most structural features left intact, is observed for the Rb analog of chlorothionite.

On the other hand, the minerals and synthetic framework compounds of the $\text{A}_2\text{Cu}(\text{SO}_4)_2$ series demonstrate a vivid example of morphotropism with the formation of structural types depending on the size of the cations residing in the cavities of the $[\text{Cu}(\text{SO}_4)_2]^{2-}$ open-framework. To date, four versions can be distinguished (Table 3). We propose to call this series of compounds “saranchinaite-type”, since for the first time such stoichiometry $[\text{M}_2\text{Cu}(\text{SO}_4)_2]$ was revealed during the discovery and description of saranchinaite $\text{Na}_2\text{Cu}(\text{SO}_4)_2$ (Siidra et al. 2018) and shortly thereafter its synthesized synthetic analogue (Kovrugin et al., 2019). Saranchinaite forms a framework with a unique topology (further denoted as type 1) that has not yet been identified in other anhydrous copper and alkali metal sulfates. Note the presence of only a minor admixture of potassium in one of the positions in the mineral (Siidra et al. 2018). $\text{K}(\text{Na},\text{K})\text{Na}_2[\text{Cu}_2(\text{SO}_4)_4]$ (Siidra et al., 2021) with a significant potassium content crystallizes in a completely different structure type (2). The $\text{Rb}_2\text{Cu}(\text{SO}_4)_2$ described in this work, containing only rubidium atoms, also forms a new structure type. The recently described family of compounds $\text{KMCu}(\text{SO}_4)_2$ ($M = \text{Na}, \text{K}$) (Borisov et al., 2021; Zhou et al., 2020) is substantially

supplemented by two rubidium representatives $\text{RbNaCu}(\text{SO}_4)_2$ and $\text{RbKCu}(\text{SO}_4)_2$. Attempts to obtain a solely sodium representative of this structural type (**3**) were unsuccessful. The type **3** compound with channels predominantly occupied by sodium apparently does not exist. Sodium analogues of anhydrous sulfates discussed herein, except of chlorothionite, represent their own structure types. However, euchlorine – type $A_2\text{Cu}_3\text{O}(\text{SO}_4)_3$ ($A_2 = \text{Na}_2, \text{NaK}, \text{and K}_2$) compounds (Nekrasova et al., 2020) and minerals (Vergasova et al., 1988; Siidra et al., 2017, 2019) demonstrate the same structure type. The dimensionality of Cu-SO₄ backbones may be crucial for the inclusion of Na⁺ keeping the same structure type. Framework compounds such as *e.g.* saranchinaite-type and cryptochalcite-type may show different architectures depending on the size of alkali metal, whereas *e.g.* euchlorine-type and chlorothionite-type having layered and chain structures are more flexible to include alkali metals of significantly various ionic radii.

Note that the structural architectures of anhydrous sulfates do not relate exclusively to framework ones. Thus, piypite and its synthetic analogs are based on chain copper oxide-sulfate complexes; chlorothionite and its polymorphs are also based on chain complexes formed via weak Cu-Cl bonds. The discovery of a new $\text{Rb}_2\text{Cu}(\text{SO}_4)\text{Cl}_2$ monoclinic polymorph of chlorothionite (Table 4) seems to be of particular interest considering the recently discovered interesting magnetic properties on synthetic $\text{K}_2\text{Cu}(\text{SO}_4)\text{X}_2$ ($X = \text{Cl}, \text{Br}$) (Soldatov et al., 2018; Bo et al., 2020) and $\text{Na}_2\text{Cu}(\text{SO}_4)\text{Cl}_2$ (Fujihala et al., 2020). Note that both sodium and potassium analogs are completely isostructural. An interesting pattern with a change in symmetry depending on the size of the alkaline cation is observed in the structures piypite and its synthetic analogs (Table 5). $\text{Rb}_4\text{Cu}_4\text{O}_2(\text{SO}_4)_4 \cdot (\text{Cu}^{+0.83}\text{Rb}_{0.17}\text{Cl})$ and $\text{K}_4\text{Cu}_4\text{O}_2(\text{SO}_4)_4 \cdot (\text{Na,Cu})\text{Cl}$ crystallize in $I4$ space group, while $\text{Na}_4\text{Cu}_4\text{O}_2(\text{SO}_4)_4 \cdot (M\text{Cl})$ ($M = \text{Na}, \text{Cu}, \square$) crystallizes in $P4/n$. It can be seen that filling of the channels with metal chloride ($Me\text{Cl}$) complexes shows significant variations. It should be noted that the structural features of piypite from the fumaroles of Tolbachik volcano have not been studied to date. Effenberger and Zemann (1984) explicitly state in their article that “the nature of the Me atoms is not completely clear”.

$\text{Rb}_2\text{Cu}_2(\text{SO}_4)_3$ also shows an example of crystallization in the already known structure type first observed for $\text{K}_2\text{Cu}_2(\text{SO}_4)_3$ (Lander et al., 2017). In $\text{Rb}_2\text{Cu}_2(\text{SO}_4)_3$, the unit-cell parameters increase significantly in accordance with an increase in the ionic radius of the alkali cation. The stoichiometry of the $A_2M^{2+}_2(\text{SO}_4)_3$ compounds corresponds to one of the most common potassium and magnesium sulfates - langbeinite $\text{K}_2\text{Mg}_2(\text{SO}_4)_3$, which crystallizes in the $P2_13$ cubic space group. In the fumaroles of the scoria cones of the Tolbachik volcano, langbeinite is also one of the most common anhydrous sulfates. Langbeinite-type compounds show very wide variations in isomorphic substitutions (Gattow and Zemann, 1958). The main factor for the formation of the $A_2\text{Cu}_2(\text{SO}_4)_3$ orthorhombic structure is the Jahn-Teller copper cations. In the same series of syntheses, where

$\text{Rb}_2\text{Cu}_2(\text{SO}_4)_3$ was obtained, “hydrolangbeinite” $\text{Rb}_2\text{Cu}_2(\text{SO}_4)_3(\text{H}_2\text{O})$ was found, formed as a result of a minor hydration of the initial mixture of reagents. Hydrated langbeinites are currently unknown for any composition of minerals or synthetic compounds. The obtained new compound shows the probability of detecting such compounds (especially for copper-containing ones) in the zones of fumaroles exposed to intense atmospheric precipitation. Alkali copper sulfates are known to form multiple hydrated “offsprings” during exposure to moist air (Siidra et al., 2021).

In the determined new structural architectures, a number of features were revealed which were seldom observed before. The first is the bidentate coordination of the tetrahedral sulfate group via edge sharing to the Cu^{2+} coordination polyhedron. Until recently, such coordination was known only for the chlorothionite structure. The second is formation of “high-coordinated” CuO_7 polyhedra. We considered such coordination when describing crystal structure of saranchinaite (Siidra et al. 2018). The structures of the new compounds suggest that such coordination is not in fact so uncommon, at least among anhydrous alkali copper sulfates. All of the described features clearly indicate the importance of further systematic studies of anhydrous copper-sulfate systems. Their exploration, particularly of the new copper-oxide substructures with new coordination environments, is highly likely to lead to new potentially interesting magnetic properties due to unusual arrangements of magnetically active Cu^{2+} cations. The effect of the alkali cation size on the Cu^{2+} coordination has been demonstrated recently for the family of synthetic hydrogen selenites (Charkin et al. 2019); one can expect that it will also be pronounced in other families, including sulfates.

Tables 2-5, listing the crystallographic parameters, show that anhydrous sulfates are a fruitful playground for the synthesis of new anhydrous compounds known previously only as prototype-structures in minerals. Conversely, it is highly probable that compounds, obtained so far only as synthetics, may exist as minerals in high-temperature fumaroles with strongly oxidizing conditions and in sublimates of natural coal fires (Pautov et al., 2020).

It is worth noting here that synthetic analogs of various minerals, including sulfates, have been obtained using various synthetic approaches which do not necessarily mimic the natural processes (or, more exactly, the currently adopted formation mechanisms). By now, condensation from vapor phase or interaction of hot gases with the base rocks are considered to be the most likely formation mechanisms of fumarolic minerals (REFS!). Yet, our studies clearly indicate that vapor transport in water-free systems can be neglected at least until 600°C wherein the only volatile species are copper chlorides. At least some of the species produced herein have most likely crystallized from melts. Several test experiments have shown that at least some Rb-containing compositions melt at as low temperatures as $400 - 450^\circ\text{C}$; moreover, good quality crystals and homogeneous samples were not produced even after long-time subsolidus heat treatments. Additional experiments are clearly necessary to elucidate the role of reaction kinetics in solid-state processes. The other synthetic

approach, applied successfully to preparation of analogs of chlorothionite, is crystallization from hot aqueous solutions (REFS!). However, one can expect competitive formation of less soluble double sulfates, *e.g.* Tutton salts, or hydrolysis products, *e.g.* analogs of hatrochalcite. Overall, the chemistry of hydrates with low water content remains in many respects a *terra incognita*. A possible solution lies in exploiting media with low chemical potential of water; our current example is the $\text{Rb}_2\text{Cu}_2(\text{SO}_4)_3 \cdot \text{H}_2\text{O}$, formed under low pressure of water vapors (given the sealed tube had survived internal pressure upon annealing). A test experiment with the initially wet sulfate charge annealed in a temperature gradient between ambient and 650°C produced good quality single crystals of various known hydrates including $\text{CuSO}_4 \cdot 5\text{H}_2\text{O}$ in the relatively cold part of the sealed silica tube. Therefore, this approach is promising in producing various hydrates hardly accessible in any other way. The use of moist non-aqueous solvents seems to be not straightforward as they either do not dissolve most inorganic sulfates (alcohols) or coordinate competitively to copper (acetonitrile). The process involving water evidently take place also under natural conditions, *e.g.* upon hydration-dehydration cycles. Yet, our studies of such processes for selected copper sulfate minerals indicate that these are very complicated, include numerous steps and are not always reversible even for single-phase specimens. It is however very likely that these studies, extended into more complex systems, will produce even more intricate and intriguing architectures, compositions, and possibly properties. Some of these studies are now in progress.

Acknowledgements

We are grateful to XXX for valuable comments. Technical support by the SPbSU X-ray Diffraction Resource Centre is gratefully acknowledged.

References

Bo X., Wang D., Wan B., and Wan X.G. (2020) Calculated magnetic exchange interactions in the quantum spin chain materials $\text{K}_2\text{CuSO}_4\text{Cl}_2$ and $\text{K}_2\text{CuSO}_4\text{Br}_2$. *Physical Reviews*, *B101*, 024416.

Bruker-AXS (2014) APEX2. Version 2014.11-0. Madison, Wisconsin, USA.

Burns P.C. and Hawthorne, F.C. (1995) Coordination geometry pathways in Cu^{2+} oxysalt minerals. *Canadian Mineralogist*, **33**, 889-905.

Charkin D.O., Markovski M.R., Siidra O.I., Nekrasova D.O. and Grishaev V.Yu. (2019) Influence of the alkali cation size on the Cu^{2+} coordination environments in $(\text{AX})[\text{Cu}(\text{HSeO}_3)_2]$ (A = Na, K, NH_4 , Rb, Cs; X = Cl, Br) layered copper hydrogen selenite halides. *Zeitschrift für Kristallographie - Crystalline Materials*, **234**, 739-747.

Effenberger H. and Zemann J. (1984) The crystal structure of caratiite. *Mineralogical Magazine*, **48**, 541-546.

Fujihala M., Mitsuda S., Mole R.A., Yu D.H., Watanabe I., Yano S., Kuwai T., Sagayama H., Kouchi T., Kamebuchi H. and Tadokoro M. (2020) Spin dynamics and magnetic ordering in the quasi-one-dimensional $S=1/2$ antiferromagnet $\text{Na}_2\text{CuSO}_4\text{Cl}_2$. *Physical Reviews*, **B101**, 024410.

Gattow G. and Zemann J. (1958) Über Doppelsulfatsalze vom Typ $A^+_2B^{2+}_2(\text{SO}_4)_3$. *Zeitschrift für Anorganische und Allgemeine Chemie*, **293**, 233-240.

Giacovazzo C. Scandale E. and Scordari F. (1976) The crystal structure of chlorothionite $\text{CuK}_2\text{Cl}_2\text{SO}_4$. *Zeitschrift für Kristallographie - Crystalline Materials*, **144**, 226-237.

Hawthorne F.C., Krivovichev S.V. and Burns P.C. (2000) The crystal chemistry of sulfate minerals. In Sulfate Minerals – Crystallography, Geochemistry and Environmental Significance (C.N. Alpers, J.L. Jambor, D.K. Nordstrom, eds.). Mineralogical Society of America and Geochemical Society, *Reviews in Mineralogy and Geochemistry*, **40**, 1-112.

Kahlenberg V., Piotrowski A. and Giester G. (2000) Crystal structure of $\text{Na}_4[\text{Cu}_4\text{O}_2(\text{SO}_4)_4]\cdot\text{MeCl}$ (Me: Na, Cu, vac) - the synthetic Na-analogue of piypite (caratiite). *Mineralogical Magazine*, **64**, 1099-1108.

Kornyakov I.V., Vladimirova V.A., Siidra O.I. and Krivovichev S.V. (2021) Expanding the averievite family, $(MX)\text{Cu}_5\text{O}_2(T^{5+}\text{O}_4)_2$ ($T^{5+} = \text{P, V}$; $M = \text{K, Rb, Cs, Cu}$; $X = \text{Cl, Br}$): synthesis and single-crystal X-ray diffraction study. *Molecules*, **26**, 833.

Marsh R.E. (1995) Some thoughts on choosing the correct space group. *Acta Crystallographica*, **B51**, 897-907.

Masquelier C. and Croguennec L. (2013) Polyanionic (phosphates, silicates, sulfates) frameworks as electrode materials for rechargeable Li (or Na) Batteries. *Chemical Reviews*, **113**, 6552-6591.

Nekrasova D.O., Tsirlin A.A., Colmont M., Siidra O.I., Vezin H. and Mentré O. (2020) Magnetic hexamers interacting in layers in the $(\text{Na,K})_2\text{Cu}_3\text{O}(\text{SO}_4)_3$ minerals. *Physical Reviews*, **B102**, 184405.

Pautov L.A., Mirakov M.A., Siidra O.I., Faiziev A.R., Nazarchuk E.V., Karpenko V.Yu. and Makhmadsharif S. (2020) Falgarite, $\text{K}_4(\text{VO})_3(\text{SO}_4)_5$, a new mineral from sublimates of a natural underground coal fire at the tract of Kukhi-Malik, Fan-Yagnob coal deposit, Tajikistan. *Mineralogical Magazine*, **84**, 455-462.

Pekov I.V., Zubkova N.V., Agakhanov A.A., Pushcharovsky D.Yu., Yapaskurt V.O., Belakovskiy D.I., Vigasina M.F., Sidorov E.G. and Britvin S.N. (2018) Cryptochalcite, $\text{K}_2\text{Cu}_5\text{O}(\text{SO}_4)_5$, and cesiodymite, $\text{CsKCu}_5\text{O}(\text{SO}_4)_5$, two new isotypic minerals and the K-Cs isomorphism in this solid-solution series. *European Journal of Mineralogy*, **30**, 593-607.

Rousse G. and Tarascon J.-M. (2014) Sulfate-based polyanionic compounds for Li-ion batteries: synthesis, crystal chemistry, and electrochemistry aspects. *Chemistry of Materials*, **26**, 394-406.

Scordari F. and Stasi F. (1990) The crystal structure of euchlorine, $\text{NaKCu}_3\text{O}(\text{SO}_4)_3$, Locality: Vesuvius, Italy. *Neues Jahrbuch für Mineralogie Abhandlungen*, **161**, 241-253. Sheldrick G.M. Crystal structure refinement with SHELXL. (2015). *Acta Crystallographica*, **B71**, 3-8.

Siidra O.I., Nazarchuk E.V., Zaitsev A.N., Lukina E.A., Avdontseva E.Y., Vergasova L.P., Vlasenko N.S., Filatov S.K., Turner R. and Karpov G.A. (2017) Copper oxosulphates from fumaroles of Tolbachik Vulcano: puninite, $\text{Na}_2\text{Cu}_3\text{O}(\text{SO}_4)_3$ - a new mineral species and structure refinements of kamchatkite and alumoklyuchevskite. *European Journal of Mineralogy*, **29**, 499-510.

Siidra O.I., Kozin M.S., Depmeier W., Kayukov R.A. and Kovrugin V.M. (2018) Copper – lead selenite bromides: A new large family of compounds partly having Cu^{2+} substructures derivable from Kagome-nets. *Acta Crystallographica*, **B74**, 712-724.

Siidra O.I., Borisov A.S., Lukina E.A., Depmeier W., Platonova N.V., Colmont M. and Nekrasova D.O. (2019) Reversible hydration/dehydration and thermal expansion of euchlorine, ideally $\text{KNaCu}_3\text{O}(\text{SO}_4)_3$. *Physics and Chemistry of Minerals*, **46**, 403-416.

Siidra O.I., Nazarchuk E.V., Agakhanov A.A. and Polekhovskiy Yu.S. (2019) Aleutite $[\text{Cu}_5\text{O}_2](\text{AsO}_4)(\text{VO}_4) \cdot (\text{Cu}_{0.5}\square_{0.5})\text{Cl}$, a new complex salt-inclusion mineral with Cu^{2+} substructure derived from Kagome-net. *Mineralogical Magazine*, **83**, 847-853.

Siidra O.I., Nazarchuk E.V., Zaitsev A.N. and Shilovskikh V.V. (2020) Majzlanite, $\text{K}_2\text{Na}(\text{ZnNa})\text{Ca}(\text{SO}_4)_4$, a new anhydrous sulphate mineral with complex cation substitutions from Tolbachik volcano. *Mineralogical Magazine*, **84**, 153-158.

Siidra O.I., Borisov A.S., Charkin D.O., Depmeier W. and Platonova N.V. (2021) Evolution of fumarolic anhydrous copper sulfate minerals during successive hydration/dehydration. *Mineralogical Magazine*, **85**, 262-277.

Soldatov T.A., Smirnov A.I., Povarov K.Yu., Hälg M., Lorenz W.E.A. and Zheludev A. (2018) Spin gap in the quasi-one-dimensional $S=1/2$ antiferromagnet $\text{K}_2\text{CuSO}_4\text{Cl}_2$. *Physical Reviews*, **B98**, 144440.

Vergasova L.P., Filatov S.K., Serafimova E.K. and Stalova G.L. (1984) Piypite $\text{K}_2\text{Cu}_2\text{O}(\text{SO}_4)_2$ - a new mineral of volcanic sublimates. *Doklady USSR Academy of Sciences, Earth Science Sections*, **275**, 714-717.

Zhou H.A., Liu Z., Ang S.S. and Zhang J.-J. (2020) Synthesis, structure, and electrochemical performances of a novel three-dimensional framework $\text{K}_2[\text{Cu}(\text{SO}_4)_2]$. *Solid State Sciences*, **100**, 106104.

Vergasova L.P., Filatov S.K., Serafimova Y.K. and Starova G.L. (1988) Fedotovite $K_2Cu_3O(SO_4)_3$ - a new mineral from volcanic sublimates. *Doklady Akademii Nauk SSSR*, **299**, 961-964.

Vergasova L.P., Starova G.L., Filatov S.K. and Anan'ev V.V. (1998) Averievite $Cu_5(VO_4)_2O_2 \cdot nMX$ - a new mineral of volcanic exhalations. *Doklady Akademii Nauk*, **359**, 804-807.

Vergasova L.P. and Filatov S.K. (2012): New mineral species in products of fumarole activity of the Great Tolbachik Fissure Eruption. *Journal of Volcanology and Seismology*, **6**, 281-289.

Table 1. Crystallographic data for Rb₂Cu(SO₄)₂, RbNaCu(SO₄)₂, RbKCu(SO₄)₂, Rb₂Cu₂(SO₄)₃, Rb₂Cu₂(SO₄)₃(H₂O), Rb₂Cu(SO₄)Cl₂, Rb₄Cu₄O₂(SO₄)₄·(Cu⁺_{0.83}Rb_{0.17}Cl), Rb₂Cu₅O(SO₄)₅.

	Rb ₂ Cu(SO ₄) ₂	RbNaCu(SO ₄) ₂	RbKCu(SO ₄) ₂	Rb ₂ Cu ₂ (SO ₄) ₃	Rb ₂ Cu ₂ (SO ₄) ₃ (H ₂ O)	Rb ₂ Cu(SO ₄)Cl ₂	Rb ₄ Cu ₄ O ₂ (SO ₄) ₄ (Cu _{0.83} Rb _{0.17} Cl)	Rb ₂ Cu ₅ O(SO ₄) ₅
Crystal system	Orthorhombic	Monoclinic	Monoclinic	Orthorhombic	Monoclinic	Monoclinic	Tetragonal	Triclinic
Space group	<i>Pna</i> 2 ₁	<i>C</i> 2/ <i>c</i>	<i>C</i> 2/ <i>c</i>	<i>P</i> 2 ₁ 2 ₁	<i>P</i> 2 ₁ / <i>n</i>	<i>C</i> 2/ <i>c</i>	<i>I</i> 4	<i>P</i> -1
Unit cell dimensions								
<i>a</i> (Å)	9.2521(4)	16.034(3)	16.1865(14)	4.8359(19)	10.1158(9)	7.4645(7)	14.171(14)	10.1002(9)
<i>b</i> (Å)	10.9671(5)	9.560(2)	10.0026(9)	12.294(4)	6.1409(5)	16.0377(18)		12.4740(10)
<i>c</i> (Å)	8.9612(4)	9.170(2)	9.3923(8)	19.036(7)	20.3446(19)	7.6580(8)	4.991(5)	14.5961(11)
<i>α</i> (°)		92.792(6)	92.149(2)		103.564(2)	116.327(6)		77.227(4)
<i>β</i> (°)								81.111(4)
<i>γ</i> (°)								89.880(4)
Unit-cell volume (Å ³)	909.28(7)	1403.9(5)	1519.6(2)	1131.7(7)	1228.56(19)	821.68(15)	1002(2)	1770.9(3)
Calculated density (g·cm ⁻³)	3.116	3.472	3.341	3.441	3.267	3.245	3.695	3.694
Absorption coefficient (mm ⁻¹)	13.507	10.975	10.594	6.885	11.910	15.285	15.752	6.394
Crystal size (mm)	0.10×0.10×0.10	0.11×0.13×0.13	0.14×0.10×0.10	0.10×0.10×0.10	0.13×0.13×0.10	0.13×0.13×0.07	0.08×0.08×0.10	0.08×0.08×0.10
Data collection								
Temperature (K)	296(2)	296(2)	296(2)	296(2)	296(2)	296(2)	296(2)	296(2)
Radiation, wavelength (Å)	MoK α , 0.71073	MoK α , 0.71073	MoK α , 0.71073	MoK α , 0.71073	MoK α , 0.71073	MoK α , 0.71073	MoK α , 0.71073	MoK α , 0.71073
θ range (°)	2.880-27.999	2.481-27.992	2.394-27.635	2.748- 18.960	2.059- 27.998	2.540-27.989	2.032-30.000	1.322-26.428
<i>h</i> , <i>k</i> , <i>l</i> ranges	-12→12 -14→14 -11→11	-21→21 -12→8 -12→8	-13→20 -12→9 -12→5	-5→5 -13→13 -22→22	-13→8 -8→8 -26→26	-9→9 -21→21 -10→9	-19→19 -19→19 -7→7	-16→15 -19→19 -23→20
Total reflections collected	18965	6789	3775	5378	11103	5905	6648	68695
Unique reflections (<i>R</i> _{int})	2180 (0.04)	1698 (0.02)	1678(0.02)	1759 (0.09)	2960 (0.5)	990(0.03)	1455(0.08)	14571(0.09)
Unique reflections <i>F</i> > 4 σ (<i>F</i>)	2049	1586	1387	1296	2005	896	944	7772
Structure refinement								
Weighting coefficients <i>a</i> , <i>b</i>	0.0, 0.0000	0.0176, 5.6518	0.0271, 0.0310	0.0297, 0.0000	0.0429, 3.2731	0.0204, 1.4496	0.0000, 13.7767	0.0421, 0.0000
Data/restraints/parameters	2180/1/123	1698/0/123	1678/0/123	1759/6/174	2960/1/189	990/0/50	1455/67/81	14571/0/596
<i>R</i> ₁ [<i>F</i> > 4 σ (<i>F</i>)], <i>wR</i> ₂ [<i>F</i> > 4 σ (<i>F</i>)]	0.019, 0.043	0.019, 0.046	0.025, 0.057	0.052, 0.091	0.041, 0.091	0.019, 0.044	0.042, 0.064	0.050, 0.097
<i>R</i> ₁ all, <i>wR</i> ₂ all	0.023, 0.045	0.021, 0.047	0.036, 0.061	0.083, 0.103	0.076, 0.107	0.024, 0.046	0.088, 0.077	0.127, 0.127
Gof on <i>F</i> ²	1.009	1.105	1.077	1.014	1.012	1.038	1.041	1.004
Largest diff. peak and hole (e ⁻ Å ⁻³)	0.413, -0.331	0.600, -0.460	0.435, -0.551	0.981, -0.884	2.365, -1.352	0.577, -0.787	1.073, -0.904	2.305, -1.816

Table 2. Crystallographic parameters of known cryptochalcite-type $A_2[Cu_5O(SO_4)_5]$ compounds.

Mineral/Synthetic Formula	cryptochalcite $K_2[Cu_5O(SO_4)_5]$	cesiodymite $CsK[Cu_5O(SO_4)_5]$	synthetic $Rb_2[Cu_5O(SO_4)_5]$
Space group	<i>P</i> -1	<i>P</i> -1	<i>P</i> -1
<i>a</i> , Å	10.0045(3)	10.0682(4)	10.1002(9)
<i>b</i> , Å	12.6663(4)	12.7860(7)	12.4740(10)
<i>c</i> , Å	14.4397(5)	14.5486(8)	14.5961(11)
α , °	102.194(3)	102.038(5)	77.227(4)
β , °	101.372(3)	100.847(4)	81.111(4)
γ , °	90.008(3)	89.956(4)	89.880(4)
<i>V</i> , Å ³	1751.7(1)	1797.5(2)	1770.9(3)
<i>R</i> ₁	0.050	0.090	0.050
Reference	Pekov et al., 2018	Pekov et al., 2018	this work

Table 3. Crystallographic parameters of known saranchinaite-type $A_2[Cu(SO_4)_2]$ compounds.

Phase modification	Saranchinaite-type compounds							
	α -phase		β -phase	γ -phase				δ -phase
Mineral/Synthetic Formula	saranchinaite $Na_2[Cu(SO_4)_2]$	synthetic $Na_2[Cu(SO_4)_2]$	synthetic $K(Na,K)Na_2[Cu_2(SO_4)_4]$	synthetic $KNa[Cu(SO_4)_2]$	synthetic $K_2[Cu_2(SO_4)_2]$	synthetic $RbNa[Cu(SO_4)_2]$	synthetic $RbK[Cu(SO_4)_2]$	synthetic $Rb_2[Cu(SO_4)_2]$
Space group	<i>P</i> 2 ₁	<i>P</i> 2 ₁	<i>P</i> 2 ₁ / <i>c</i>	<i>C</i> 2/ <i>c</i>	<i>C</i> 2/ <i>c</i>	<i>C</i> 2/ <i>c</i>	<i>C</i> 2/ <i>c</i>	<i>Pna</i> 2 ₁
<i>a</i> , Å	9.0109(5)	8.9711(3)	12.5085(9)	15.9721(10)	16.0433(11)	16.034(3)	16.1865(14)	9.2521(4)
<i>b</i> , Å	15.6355(8)	15.5482(5)	9.3166(7)	9.4576(6)	9.7819(7)	9.560(2)	10.0026(9)	10.9671(5)
<i>c</i> , Å	10.1507(5)	10.1421(3)	12.7894(10)	9.0679(6)	9.2341(7)	9.170(2)	9.3923(8)	8.9612(4)
β , °	107.079(2)	107.155(1)	107.775(2)	93.6350(10)	93.2680(10)	92.792(6)	92.149(2)	
<i>V</i> , Å ³	1367.06(12)	1351.73(7)	1419.28(19)	1367.02(15)	1446.79(18)	1403.9(5)	1519.6(2)	909.28(7)
<i>R</i> ₁	0.030	0.020	0.030	0.029	0.017	0.030	0.025	0.019
Reference	Siidra et al., 2018	Kovrugin et al., 2019	Siidra et al., 2021	Borisov et al., 2021	Zhou et al., 2020	this work	this work	this work

Table 4. Crystallographic parameters of known chlorothionite-type $A_2Cu(SO_4)X_2$ compounds.

Phase modification	α -phase				β -phase
	synthetic $Na_2Cu(SO_4)Cl_2$	chlorothionite $K_2Cu(SO_4)Cl_2$	synthetic $K_2Cu(SO_4)Cl_2$	synthetic $K_2Cu(SO_4)Br_2$	synthetic $Rb_2Cu(SO_4)Cl_2$
Space group	<i>Pnma</i>	<i>Pnma</i>	<i>Pnma</i>	<i>Pnma</i>	<i>C</i> 2/ <i>c</i>
<i>a</i> , Å	7.0324(2)	7.7320(15)	7.73	7.73	7.4645(7)
<i>b</i> , Å	5.60540(10)	6.078(1)	6.08	6.30	16.0377(18)
<i>c</i> , Å	16.0344(4)	16.2920(30)	16.29	16.43	7.6580(8)
β , °					116.327(6)
<i>V</i> , Å ³	632.07(3)	765.64	765.60	800.12	821.68(15)
<i>R</i> ₁	0.0244	0.032	-	-	0.019

Reference	Fujihala et al., 2020	Giacovazzo et al., 1974	Bo et al., 2020	Bo et al., 2020	this work
-----------	-----------------------	-------------------------	-----------------	-----------------	-----------

Table 5. Crystallographic parameters of known piypite-type $\text{Rb}_4[\text{Cu}_4\text{O}_2(\text{SO}_4)_4] \cdot (M\text{Cl})$ compounds.

Phase modification	α -phase		β -phase
Mineral/Synthetic	synthetic	piypite	synthetic
Formula	$\text{Na}_4[\text{Cu}_4\text{O}_2(\text{SO}_4)_4] \cdot (M\text{Cl})$ ($M = \text{Na}, \text{Cu}, \square$)	$\text{K}_4[\text{Cu}_4\text{O}_2(\text{SO}_4)_4] \cdot (Me\text{Cl})$	$\text{Rb}_4[\text{Cu}_4\text{O}_2(\text{SO}_4)_4] \cdot (\text{Cu}^{+}_{0.83}\text{Rb}_{0.17}\text{Cl})$
Space group	$P4/n$	$I4$	$I4$
a , Å	18.451(1)	13.60(2)	14.171(14)
c , Å	4.9520(2)	4.98(1)	4.991(5)
V , Å ³	1685.86(15)	921.1	1002(2)
R_1	0.028	0.035	0.043
Reference	Kahlenberg et al. 2000	Effenberger and Zemann, 1984	this work

